

# Complete wave-vector directions of electromagnetic emissions: Application to INTERBALL-2 measurements in the nightside auroral zone

O Santolik, François Lefeuvre, Michel Parrot, Jean-Louis Rauch

▶ **To cite this version:**

O Santolik, François Lefeuvre, Michel Parrot, Jean-Louis Rauch. Complete wave-vector directions of electromagnetic emissions: Application to INTERBALL-2 measurements in the nightside auroral zone. Journal of Geophysical Research Space Physics, 2001, 106, pp.13191-13201. insu-03234754

**HAL Id: insu-03234754**
**https://insu.hal.science/insu-03234754**

Submitted on 25 May 2021

**HAL** is a multi-disciplinary open access archive for the deposit and dissemination of scientific research documents, whether they are published or not. The documents may come from teaching and research institutions in France or abroad, or from public or private research centers.

L'archive ouverte pluridisciplinaire **HAL**, est destinée au dépôt et à la diffusion de documents scientifiques de niveau recherche, publiés ou non, émanant des établissements d'enseignement et de recherche français ou étrangers, des laboratoires publics ou privés.

JOURNAL OF GEOPHYSICAL RESEARCH, VOL. 106, NO. A7, PAGES 13,191–13,201, JULY 1, 2001

# Complete wave-vector directions of electromagnetic emissions: Application to INTERBALL-2 measurements in the nightside auroral zone

O. Santolík,[1,2] F. Lefeuvre, M. Parrot, and J. L. Rauch

Laboratoire de Physique et Chimie de l'Environnement, Centre National de la Recherche Scientifique, Orléans, France.

**Abstract.** We present several newly developed methods for wave propagation analysis. They are based on simultaneous measurement of three magnetic field components and one or two electric field components. The purpose of these techniques is to estimate complete wave vector direction and the refractive index. All the analysis results are validated by well defined simulated data. Propagation analysis of natural emissions in the night-side auroral zone at high altitudes is done using the data of the MEMO (Mesures Multicomposantes des Ondes) experiment onboard INTERBALL-2. The results show that a bursty whistler mode emission propagates toward the Earth near the resonance cone. Upward propagating auroral kilometric radiation in the *R-X* mode represents another example demonstrating the potential of such analysis for future applications.

## 1. Introduction

With multicomponent wave measurement onboard satellites, the wave vector direction may be determined using the Faraday's law. Its consequence in the frequency domain is the perpendicularity of the magnetic field vector **B** to both the wave vector **k**, and the electric field vector **E**. The magnetic field data are often used to characterize **k** [e.g., *Means*, 1972; *McPherron et al.*, 1972; *Samson and Olson*, 1980]. The wave vector direction is here defined by the normal to the polarization plane of the magnetic field. If the polarization is circular or elliptic, two mutually antiparallel directions always meet this condition. The result is thus ambiguous, and the wave vector direction can only be determined in a single hemisphere. The complete wave vector direction without this ambiguity may be however determined if we measure both the magnetic field and the electric field [*Lefeuvre et al.*, 1986]. To fully define the wave vector, we also need to determine its modulus, the wave number $k$. This, again, cannot be done without considering the wave electric field components. A nonambiguous determination of the propagation characteristics of a wave is of crucial importance for the location of the source and the identification of the generation mechanism of plasma waves. In theory, it requires the measurement of six electromagnetic field components (three electric and three magnetic), and the number can be reduced to five in the case of a plane wave [*Grard*, 1968; *Shawhan*, 1970].

Sometimes, the wave propagation cannot be well described by a single direction. For instance, it is the case when foregoing and reflected waves are simultaneously observed [e.g., *Lefeuvre et al.*, 1992; *Santolík and Parrot*, 2000] or when several propagation modes coexist [e.g., *Parrot et al.*, 1989]. Then the wave propagation may be described by means of the wave distribution function (WDF) introduced by *Storey and Lefeuvre* [1979]. However, the quasi-plane wave approximation is often valid when a direction or/and a mode is dominant. Even if the field is not exactly consistent with this assumption, an estimate of the plane wave parameters may represent an average value for all simultaneously propagating waves and give a rough idea about the wave propagation.

The electric field data available from satellite measurements are often incomplete: only one or two electric components may be available. Approximations may be used for particular orientations of electric antennas as regards to the Earth magnetic field direction [*Lefeuvre et al.*, 1986]. In the other cases, specific analysis methods must be developed. The difficulty is that the electric and magnetic wave field components being related through the refractive index, i.e., through the dispersion relation, approximations valid in one region of the Clemmow-Mullaly-Allis (CMA) diagram [*Stix*, 1992] do not apply to others. This explains why techniques which have been proved to be successful for the analysis of some satellite data (e.g., techniques developed by *Santolík and Parrot* [1998, 1999] for the extremely low frequency data of the FREJA satellite) must be reexamined for other data.

In this paper, analysis techniques are used under the plane wave approximation, and for an incomplete set of data. We revise these methods in the context of the INTERBALL-

[1] Also at Faculty of Mathematics and Physics, Charles University, Prague, Czech Republic.

[2] Now at Department of Physics and Astronomy, University of Iowa, Iowa City.

Copyright 2001 by the American Geophysical Union.

Paper number 2000JA000275.
0148-0227/01/2000JA000275$09.00

2 waveform data, with a potential application to the data of the STAFF (Spatio-Temporal Analysis of Field Fluctuations) spectral analyzer onboard the European Space Agency CLUSTER satellites. Two sets of INTERBALL-2 observations made in November 1996, at nearly the same position (nightside, northern auroral region), are used as an example of investigation of propagation characteristics of bursty whistler mode emissions and auroral kilometric radiation (AKR). These emissions were mainly studied using the frequency power spectrograms in the past. We will show that multicomponent data, as recorded onboard INTERBALL 2 [*Lefeuvre et al.*, 1998], allow a more detailed analysis. Section 2 introduces the analysis methods, and in section 3 we show the results for the INTERBALL-2 data in two different frequency bands. Each case is compared with theoretical predictions adjusted to the particular experimental situation. Section 4 contains a discussion of results, and, finally, section 5 gives brief conclusions.

## 2. Analysis Methods

Analysis of electric field data in space plasmas may suffer from several problems. The first problem is the coupling impedance between the antennas and the plasma which often is poorly known and which may shift the phase or change the amplitude of the signal. These effects depend on parameters which are difficult to control on board and which are more or less well modeled. The second problem is the difficulty to install a long antenna in the direction of the satellite spin axis and so to get accurate measurements of the three components. The third problem exists if, owing to telemetry limitations, the waveform of a single electric field component is transmitted. This is the case of INTERBALL 2 data in the highest frequency band (20 – 200 kHz).

It is therefore important to have methods which (1) characterize the complex transfer function (the phase shift and the change of amplitude) directly from the wave data, (2) estimate the hemisphere of propagation to complete the wave vector direction, (3) estimate the wave number, and (4) are able to work with incomplete electric field data, i.e., with measurements of only one or two electric components. The full vector measurement of the wave magnetic field is supposed. Several methods meeting some of these points are described in this section.

The basic equation used by all the analysis methods is the Faraday's law,

$$\nabla \times \mathbf{E} = -\frac{\partial \mathbf{B}}{\partial t}. \tag{1}$$

All the methods work in the frequency domain. The multicomponent data are first subjected to a cross-spectral analysis. At each analyzed frequency, the result of this procedure is a Hermitian spectral matrix,

$$S_{ij} = \langle \mathcal{A}_i \mathcal{A}_j^* \rangle, \tag{2}$$

where $\mathcal{A}_i$ and $\mathcal{A}_j$ are the complex amplitudes of $i$th and $j$th signal obtained by a classical spectral analysis [e.g., *Priestley*, 1989], the asterisk stands for the complex conjugate, and $\langle\rangle$ mean the time average. Autopower spectra of separate signals may be found on the main diagonal of the spectral matrix. Its off-diagonal elements are complex cross spectra between each two signals, giving information about mutual phase and coherency relations.

### 2.1. Analysis Using the Magnetic Field Vector Data

Although the subject of the present paper is a simultaneous analysis of the magnetic and electric fields, we will also need three auxiliary procedures based only on the magnetic field vector measurements. Methods of direction finding with these data [e.g., *Means*, 1972; *McPherron et al.*, 1972; *Samson and Olson*, 1980] are based on the perpendicularity of the wave vector to the wave magnetic field,

$$\mathbf{B} \cdot \mathbf{k} = 0, \tag{3}$$

which is is a consequence of (1) in the frequency domain. In this paper we will use the method of *Means* [1972]. It consists of a straightforward algebraic expression using imaginary parts of three magnetic cross spectra and gives estimates of angles $\theta$ and $\phi$ which characterize the wave vector direction in a spherical coordinate system. Owing to the ambiguity noted in section 1, we cannot distinguish two opposite directions. We may thus choose to represent the results in the hemisphere where $\theta \leq 90°$. It is also useful to transform the wave magnetic data into a system whose $z$ axis is parallel to the ambient magnetic field ($\mathbf{B}_0$). Obviously, this transformation needs the full vector measurements. Polar angle $\theta$ then defines the angle deviation from the ambient DC magnetic field, and angle $\phi$ gives the azimuth having the zero value in the direction of increasing magnetic latitude. The method always gives an ambiguous result with $\theta \leq 90°$, which may also indicate an antiparallel propagation with $\theta' = 180° - \theta$ and $\phi' = 180° + \phi$.

We will also use an estimate of the sense of circular or elliptical polarization in the plane perpendicular to $\mathbf{B}_0$,

$$C_B = \frac{\Im S_{xy}}{\sigma(\Im S_{xy})}, \tag{4}$$

where $\Im S_{xy}$ is the imaginary part of the cross spectrum between the two perpendicular magnetic components, and $\sigma(\Im S_{xy}) = \sqrt{(S_{xx}S_{yy} - \Re S_{xy}^2 + \Im S_{xy}^2)}/\sqrt{(2M)}$ is an estimate of its standard deviation [*Priestley*, 1989]. Here, $\Re S_{xy}$ is the real part of this cross spectrum, $S_{xx}$ and $S_{yy}$ are the corresponding autospectra, and $M$ is the number of matrices entering into the average in (2). With the convention we use for the spectral analysis, negative values of $C_B$ mean left-hand polarized waves (sense of the gyration of ions) and positive values correspond to right-handed polarization (sense of the gyration of electrons). The absolute value gives the level of confidence, and values above 3 or below −3 generally indicate a high confidence level.

The underlying hypothesis on the presence of a single plane wave will be tested by an estimator of the degree of polarization obtained by the eigenanalysis of the spectral matrix [*Samson*, 1977; *Storey et al.*, 1991; *Lefeuvre et al.*, 1992],

$$P = \frac{V_3}{V_1 + V_2 + V_3}, \quad (5)$$

where $V_1$, $V_2$, and $V_3$ are three real eigenvalues of the spectral matrix $3\times3$ of the three magnetic components, $V_3$ being the largest one. A value above $\sim$0.8 means that the wave magnetic field approximately corresponds to that of a single plane wave.

### 2.2. Estimations From the Magnetic Field Vector Data and a Single Electric Signal

As noted in section 1, the two opposite wave vector directions may be distinguished if we use both magnetic and electric field data. We must obviously know the direction of the electric antenna in the coordinate system, which is used for the components of the wave magnetic field vector data, i.e., in the $\mathbf{B_0}$ frame. Even if more than one electric antenna is available, it can be useful to check that similar results are independently obtained for each electric signal. With a single electric antenna, two approximate methods can be used.

The first possibility is to determine the phase shift between the electric signal and a magnetic component $B_a = \mathbf{p_a} \cdot \mathbf{B}$. This component is calculated as a projection of the magnetic field vector to a unit vector $\mathbf{p_a} = \hat{\mathbf{z}} \times \mathbf{a}$, perpendicular to both a unit vector $\mathbf{a}$ in the direction of the electric antenna and the $z$ axis of the $\mathbf{B_0}$ coordinate system [*Santolík and Parrot*, 1999]. Using the cross spectrum $S_{xa}$ between the $x$ component of the magnetic field and the electric signal (i.e., the component of the electric field along the antenna axis), together with the cross spectrum $S_{ya}$ between the magnetic $y$ component and the same electric signal, we have

$$\begin{aligned} S_{Ba} &= (\Re S_{xa} a_y - \Re S_{ya} a_x) + i(\Im S_{xa} a_y - \Im S_{ya} a_x) \\ &= |S_{Ba}| \exp(i\Phi_a), \end{aligned} \quad (6)$$

where $a_x$ and $a_y$ are two components of the vector $\mathbf{a}$ in the $\mathbf{B_0}$ coordinate system. The phase shift is then defined by the complex phase $\Phi_a$ of the complex scalar quantity $S_{Ba}$. Generally, $\Phi_a$ may have any value depending on the actual orientation of the antenna, on the unknown wave vector, and on the wave mode. In two special cases, however, $\Phi_a$ directly reflects the hemisphere of $\mathbf{k}$: first, when the antenna direction lies in the plane perpendicular to $\mathbf{k}$, and second, when the parallel component of the wave electric field ($E_z$) is negligible. In those cases, the phase shift $\Phi_a$ is either 0° or 180°: A phase shift around 180° corresponds to a positive $z$ component of the wave vector $k_z$ ($\theta < 90°$), and the zero value corresponds to a negative $k_z$ ($\theta > 90°$). If the procedure is continuously applied to the data of a spinning electric antenna, there are at least two points where the antenna intersects the plane perpendicular to $\mathbf{k}$. If we know the $\mathbf{k}$ direction (e.g., from the method of *Means* [1972]) or if we are able to identify these points from the resulting time series, then in both these points we obtain $\Phi_a$ either 0° or 180°, and we can determine the hemisphere of propagation. Sometimes we can use this method continuously because of a negligible $E_z$. This is true for some combinations of wave mode, frequency, and/or wave vector direction (for example, the whistler mode emissions presented by *Santolík and Parrot* [1999]). Note that the transfer function of the antenna-plasma interface may have a nonzero imaginary part. In such a case it induces a phase shift to the electric signal. This phase shift is then directly reflected by $\Phi_a$ as an additive value. This may complicate the analysis, but under some circumstances the method may also serve to estimate the unknown transfer function.

If the electric field vector is parallel to the antenna direction, the above procedure might also be used in the determination of the sign of the $z$ component of the Poynting vector ($F_z$). Another, closely related, method may be used to estimate $F_z$ normalized by its standard deviation, $D = F_z/\sigma(F_z)$. With a single electric antenna we would obtain $D$ only if the electric field vector were parallel to the antenna direction. We can however make use of an approximate estimation from real parts of the cross spectra between the electric signal and two perpendicular magnetic components [*Santolík and Parrot*, 1998, 1999],

$$D_a = \frac{\Re S_{ya} a_x - \Re S_{xa} a_y}{\sigma(\Re S_{ya})|a_x| + \sigma(\Re S_{xa})|a_y|}, \quad (7)$$

where $\sigma(\Re S_{ya})$ and $\sigma(\Re S_{xa})$ are estimates of the standard deviations of the respective cross spectra [*Priestley*, 1989]. Note that the "direction indicator" of *Santolík and Parrot* [1998] was defined in that way that it is equivalent to $-D_a$. Here, positive values of $D_a$ correspond to a positive $z$ component of the Poynting vector. The absolute value of $D_a$ indicates the reliability of the result. If it is higher than 3, the interpretation of $D_a$ in terms of the sign of $F_z$ is statistically reliable. All remarks made above concerning the interpretation of $\Phi_a$ for the estimation of the $k_z$ sign are also valid here.

### 2.3. Analysis Using the Magnetic Field Vector Data and Two Electric Signals

With two electric antennas we can easily extend the preceding method. We again suppose that we dispose of three magnetic components in the $\mathbf{B_0}$ frame and that in this frame we also know unit vectors $\mathbf{a_1}$ and $\mathbf{a_2}$ defining the directions of the two electric antennas. These directions may or may not be mutually orthogonal. An extension of (7) then reads

$$D_b = \frac{\sum_i (\Re S_{yi} a_{ix} - \Re S_{xi} a_{iy})}{\sum_i \left[\sigma(\Re S_{yi})|a_{ix}| + \sigma(\Re S_{xi})|a_{iy}|\right]}, \quad (8)$$

where the index $i$ goes from 1 to 2, for the first and the second electric antenna, respectively. Equation (8) represents the sum of separate $F_z$ estimates from (7) normalized by the sum of their standard deviations. This method gives an exact value of $F_z/\sigma F_z$ in the special case of two orthogonal electric antenna in the plane $x$-$y$ (perpendicular to $\mathbf{B_0}$). The result indicates the correct sign of $k_z$ if $k_z(S_{11} + S_{22}) > \Re S_{Ez1} k_1 + \Re S_{Ez2} k_2$, where $S_{11}$ and $S_{22}$ are the two electric autospectra, $\Re S_{Ez1}$ and $\Re S_{Ez2}$ are real parts of hypothetical electric crosspectra with the $E_z$ com-

ponent and $k_1$, $k_2$ are the projections of the wave vector to the directions of the two antennas. This condition is always valid if $E_z$ is negligible but also in other cases depending on $E_z$, $k_1$, and $k_2$. Otherwise, interpretation of $D_b$ is similar as in the case of $D_a$. Note also that a further extension of (8) for three orthogonal electric antennas may be obviously done by adding the third antenna to the sum, taking $i = 1 \ldots 3$. In this case, $D_b$ would always give the right value of $F_z/\sigma(F_z)$, independently of the directions of antennas, the wave vector, and the wave electric field. This method is thus important because of a relatively simple procedure and because it represents an intermediate step between the method (7) for a single antenna and a universal procedure for three orthogonal electric antennas.

However, with two electric antennas we can use another method to distinguish the two antiparallel wave vector directions without any assumption on the wave mode or on the actual directions of antennas. At the same time we can estimate the wave number. As a consequence of (1) in the frequency domain, we have

$$n\,(\boldsymbol{\kappa} \times \mathbf{E}) = c\mathbf{B}, \tag{9}$$

where $n$ is the index of refraction $n = k\,c/\omega$, $c$ is the speed of light, $\omega$ is the angular frequency, and $\boldsymbol{\kappa}$ is a unit vector parallel to the wave vector direction $\boldsymbol{\kappa} = \mathbf{k}/k$. If we know $\boldsymbol{\kappa}$, we can use it in (9) to estimate $n$ (and then the wave number $k$) from the measured electric and magnetic fields. Before using in (9), $\boldsymbol{\kappa}$ may be determined by a method based on (3), for example by the method of *Means* [1972]. As such calculation does not distinguish the two antiparallel wave vector directions, we have two possibilities: either the correct $\boldsymbol{\kappa}$ is introduced in (9), or $-\boldsymbol{\kappa}$ is used. In the latter case, we obtain $-n$ instead of $n$, and, as $n$ cannot be negative, we may use (9) to resolve the sign ambiguity of $\boldsymbol{\kappa}$.

The vector equation (9) may be written as three scalar equations in a Cartesian frame. Each equation necessarily contains two electric components from the vector product on the left-hand side. With two electric antennas we may use one of these scalar equations to determine $n$,

$$n = cB_{z'} \,/\, (\kappa_{x'} E_{y'} - \kappa_{y'} E_{x'}). \tag{10}$$

The principal step of this method is thus the transformation of the three-component magnetic field data to get the $B_{z'}$ component in a Cartesian frame connected with the electric antennas. The $x'$ axis of this frame is parallel with a unit vector $\mathbf{a}_1$ in the direction of the first antenna. Its $z'$ axis is parallel to a unit vector $\hat{\mathbf{z}}' = \mathbf{a}_1 \times \mathbf{a}_2$, perpendicular to both antennas. The $y'$ axis completes the right-handed Cartesian system, lying in the plane of the two antennas. The component $E_{y'}$ then reads $E_{y'} = (E_2 - E_1 \cos\alpha)/\sin\alpha$, where $\cos\alpha = \mathbf{a}_1 \cdot \mathbf{a}_2$ characterizes the angle between the directions of antennas. $E_1$ and $E_2$ are the projections of the electric field vector to the directions of the two antennas, respectively. We always have $E_{x'} = E_1$, and if the antennas are mutually orthogonal, we also have $E_{y'} = E_2$.

Experimental measurements of the electric field may be influenced by a transfer function of the antenna-plasma interface. As we will make use of such data in (10), we must take into account this transfer function. Suppose that the $i$th recorded electric signal $\mathcal{E}_i$ may be written in the frequency domain as $\mathcal{E}_i = Z\,E_i$, where $Z$ is a complex transfer function at a given frequency (the same for all the antennas) and $E_i$ is a theoretical electric component in the direction of the $i$th antenna. Then if we use experimental data in (10), we have a complex value $N = n/Z$ on the left-hand side. Equation (10) may be finally rewritten to obtain an estimate of $N$ from the components of a spectral matrix,

$$N = \frac{c\left(S_{xj}\hat{z}'_x + S_{yj}\hat{z}'_y + S_{zj}\hat{z}'_z\right)}{\kappa_{x'}\left[(S_{2j} - S_{1j}\cos\alpha)/\sin\alpha\right] - \kappa_{y'}S_{1j}}, \tag{11}$$

where $\hat{z}'_x$, $\hat{z}'_y$, and $\hat{z}'_z$ are Cartesian components of $\hat{\mathbf{z}}'$ in the original frame of the magnetic components, $S_{xj}$, $S_{yj}$, and $S_{zj}$ are the cross spectra or autospectra between the magnetic components $B_x$, $B_y$, and $B_z$ and a fixed magnetic component ($j$ is either $x$ or $y$ or $z$), and, finally, $S_{1j}$ and $S_{2j}$ are the cross spectra between the electric signals and the fixed magnetic component. The fixed component $j$ may be arbitrarily chosen between the three possibilities. Theoretically, the result should be the same whatever is the choice of $j$. In practice, a good choice to avoid numerical instabilities is to select $j$ which gives the largest denominator in (11).

The resulting $N$ may be decomposed to the complex amplitude and phase,

$$N = \frac{n}{|Z|}\,e^{-i\Phi_b}. \tag{12}$$

This shows that the wave refractive index cannot be separated from the absolute value of the transfer function $|Z|$, and we can only get a ratio of the two values from $|N|$. The problem is that $Z$ is often very poorly known, but in some cases, we can suppose that $|Z|$ is unity. The value of $|N| = n/|Z|$ then directly gives index of refraction $n$. At a given frequency $f$ ($f = \omega/2\pi$), it also defines the wavelength of observed electromagnetic waves, $\lambda = c/nf$.

If $|Z|$ is unknown, we can make use of theoretical values of the refractive index, and the transfer function (and thus the impedance of the electric antennas) may be estimated. Supposing that $n$ has no imaginary part, the phase $\Phi_b$ directly reflects the phase shift due to the transfer function. As a secondary effect, this value may be used to resolve the sign ambiguity of $\boldsymbol{\kappa}$, as discussed above. Values below -90° or above +90° are equivalent to a negative real part of $N$. In this case, either the phase shift introduced by the transfer function is really so high and we use the right sign of $\boldsymbol{\kappa}$ in (11), or the phase shift should be reduced by 180° and $\boldsymbol{\kappa}$ has the opposite sign. If we have a reason to suppose that the antenna-plasma interface does not modify the phase by more than 90°, we may use the latter possibility to determine the sign of $\boldsymbol{\kappa}$.

Returning to (9) we may note that in the frequency domain, the vectors of wave electric and magnetic fields are perpendicular. This property may be used to determine the full electric field vector from the measurement of three magnetic and two electric components. The procedure must

again be based on the transformation to a coordinate frame defined by the two electric antennas and is described in appendix A. In this paper we use such completed information about the wave electric and magnetic fields with two analysis methods. The first one is an extension of the above method to estimate the normalized parallel component of the Poynting vector (the $D_b$ parameter from (8), where the index $i$ goes from 1 to 3). Its application to the three orthogonal electric components makes unnecessary all the additional conditions of validity. The second method is based on a direct calculation of the angle deviation of the Poynting vector $\mathbf{F}$ from $\mathbf{B}_0$. This angle is obtained without any ambiguity, i.e. with values between 0° and 180°.

All the above presented data analysis methods are contained in the computer program PRASSADCO [*Santolík*, 2000], which is being prepared for the STAFF-SA devices onboard the CLUSTER satellites. The results shown in the present paper have been obtained by this program.

## 3. Application to the MEMO Data in Two Different Frequency Bands

The MEMO experiment [*Lefeuvre et al.*, 1998] onboard the INTERBALL project measures the waveforms of several components of the electromagnetic field. In its ELF and VLF bands (0.05-1 kHz and 1-20 kHz, respectively) it simultaneously records the data from three magnetic antennas and two electric antennas. In its HF band (20-200 kHz) it measures waveforms of three magnetic antennas and one electric antenna. We have selected two cases which will be analyzed with the above described methods. The data were respectively recorded in the ELF and HF bands of the MEMO device.

### 3.1. Analysis of a Bursty Whistler-Mode ELF Emission

The first case was recorded in the ELF band on November 12, 1996. Figure 1 shows a time-frequency spectrogram of one of the electric components measured between 1614 and 1625 UT. The data were organized in short snapshots of 1.92 s separated by ~63-s data gaps, and Figure 1 represents 10 snapshots separated by vertical lines. The satellite was at an altitude of 18,300 km in the nightside northern auroral sector at an invariant latitude of 68.5° and around 0430 MLT (magnetic local time). In the ninth snapshot of this sequence, two similar bursts of natural waves were observed at frequencies around 700 Hz. Principal characteristics of the wave propagation are shown in Figures 2a–2h.

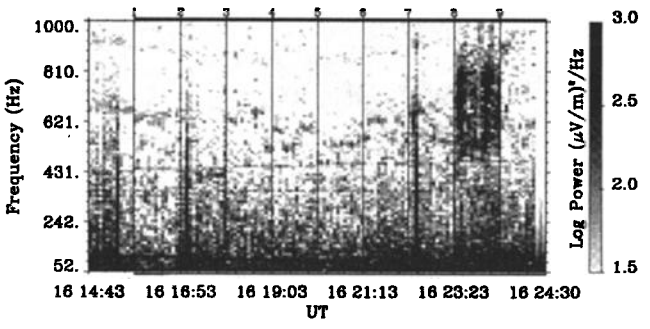



**Figure 1.** Power spectrogram of ten snapshots of the electric field data recorded in the ELF band on November 12, 1996.

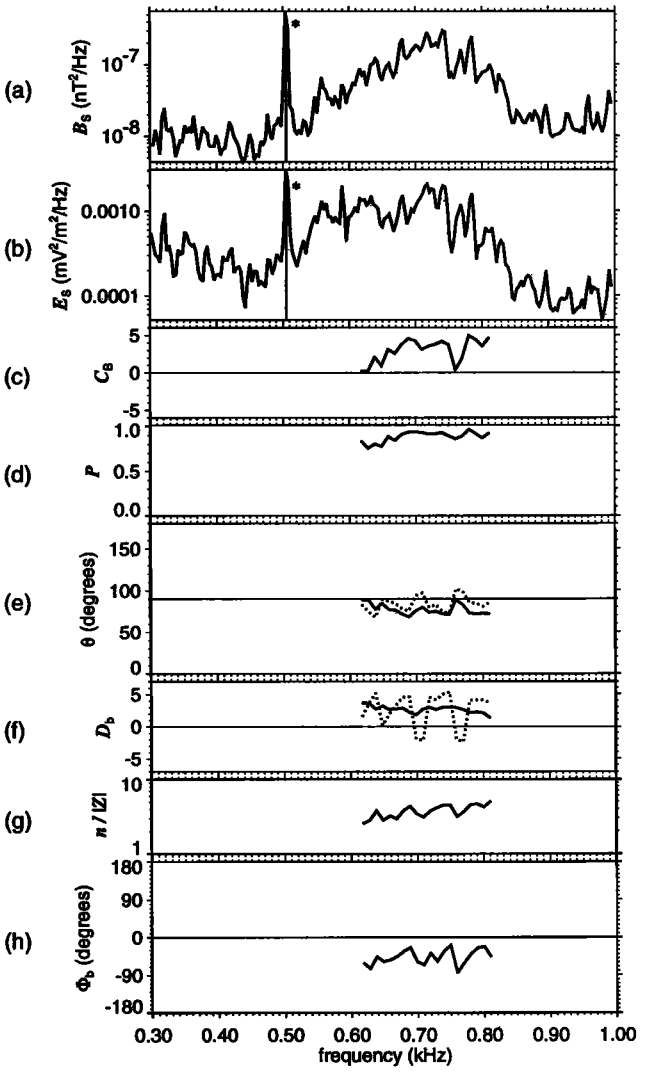



**Figure 2.** Analysis of a bursty ELF emission from November 12, 1996, 1623:23 UT, in a frequency interval 0.3 – 1 kHz. (a) Sum of the three magnetic autopower spectra. (b) Sum of the two electric autopower spectra. (c) Sense of polarization from (4). (d) Degree of polarization from (5). (e) Solid line indictes deviation $\theta$ of the wave vector direction from the ambient magnetic field $\mathbf{B}_0$ by the method of *Means* [1972] and dotted line indicates the same angle for the Poynting vector obtained from (A4). (f) Solid line denotes estimate of the normalized parallel component of the Poynting vector from (8) and dotted line denotes the same estimate using an extension of (8) for three electric components obtained using (A3). (g) Ratio of the wave refractive index and the transfer function from (12). (h) Phase shift due to the transfer function from (12).

Note that the vertical lines with asterisks in the frequency spectra (Figures 2a and 2b) identify disturbing interference signals with no relation to the observed phenomenon. These interferences are not seen in the electric component which is shown in Figure 1. The analysis is done only if the magnetic

field of the natural emission is sufficiently above the noise level (a threshold of $6\times10^{-8}$ nT$^2$/Hz is applied). Figure 2c reveals that the wave magnetic field is right-hand elliptically polarized consistent with propagation in the whistler mode. The wave magnetic field also has a relatively high polarization degree (Figure 2d) suggesting that the propagation may be well described by a single plane wave.

The main results of wave vector determination in Figures 2e–2h may be characterized by a nearly perpendicular wave vector direction with $\theta$ between 70° and 80° and with $n/|Z| = 4 - 5$. The angle azimuth $\phi$ of the wave vector obtained at the same time by the method of *Means* [1972] is ~60°, which suggests that the waves propagate from the nightside sector (from lower MLT) and from lower magnetic latitudes (not shown). The estimate of $D_b$ with the two electric antennas shows positive parallel component of the Poynting vector, which indicates that the waves are propagating toward the Earth. The estimate of $\Phi_b$ confirms this result because obtained values are generally found between -90° and 0°, but the fluctuations in the examined frequency band are very high. However, the direction of the Poynting vector is also found at very large angles with respect to $\mathbf{B_0}$, at some frequencies fluctuating above +90°. This corresponds to the results for $D_b$ obtained with the reconstructed electric field vector, where we see excursions to negative values. These contradictory features need to be analyzed before conclusions on the wave propagation properties may be done.

We have thus calculated theoretical properties of whistler mode waves at 700 Hz using the cold plasma theory [*Stix*, 1992]. The electron gyrofrequency $f_g$=23.8 kHz has been derived from the measurement of the DC magnetic field. The plasma frequency $f_p$ is supposed to be ~10 kHz following values observed at a similar position. If we suppose a plasma with 100% of hydrogen ions, the local lower hybrid frequency is 215 Hz, and at 700 Hz, the whistler mode has an oblique resonance at $\theta_R = 86°$. The wave vector cannot thus be inclined from $\mathbf{B_0}$ by more than 86°. Additionally, the Poynting vector cannot be inclined from $\mathbf{B_0}$ by more than 16°, the Gendrin angle being at $\theta_G = 80°$. This is in a clear contradiction with the results we have obtained in Figure 2 for the Poynting vector direction.

We have therefore verified these results by analysis of simulated data. We have supposed a whistler mode wave with a wave vector at $\theta = 75°$ and $\phi = 60°$, and we have used the cold plasma theory to calculate the field components in the $\mathbf{B_0}$ frame. After their projection to the known directions of antennas, we have obtained a very low power of the signal predicted for one of the electric antennas, by ~2 orders lower than the power predicted for the other antenna. Similar difference is also seen in the experimental data. As the weaker signal may be influenced by a broadband background noise, we have simulated its influence on the obtained results. We have calculated the theoretical waveforms for the above described whistler wave at 700 Hz, and we have added a white Gaussian noise generated as a pseudorandom sequence. Different noise levels have been defined by the ratio of the modulus of the magnetic or electric field vector to the standard deviation of the Gaussian noise (signal-to-noise ratio, SNR).

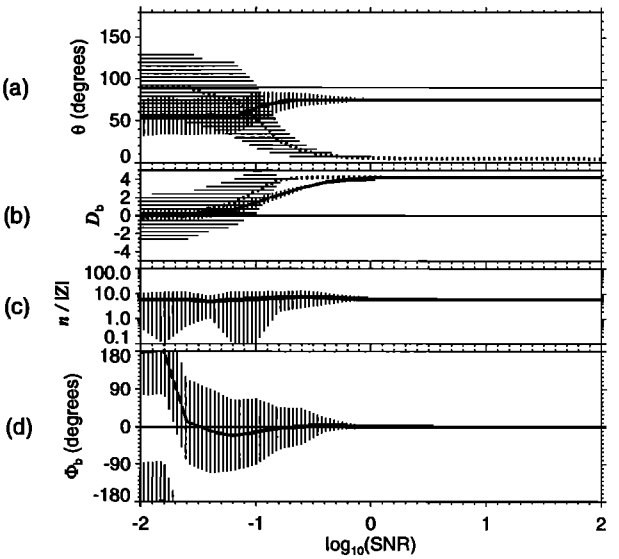



**Figure 3.** Analysis of the noise influence for the ELF case on November 12, 1996. Simulated analysis results are plotted as a function of the common logarithm of the signal-to-noise ratio. (a) Solid line indicates deviation $\theta$ of the wave vector direction from the ambient magnetic field $\mathbf{B_0}$ by the method of *Means* [1972] and dotted line indicates the same angle for the Poynting vector. (b) Solid line denotes estimate of the parallel component of the Poynting vector normalized by its standard deviation from (8) and dotted line denotes the same estimate using an extension of (8) for three electric components. (c) Ratio between the wave refractive index and the transfer function from (12). (d) Phase shift due to the transfer function from (12). The results are averaged from 100 independent realizations of the data. Regions filled by vertical lines (for the solid-line plots) or horizontal lines (for the dotted-line plots) show standard deviations estimated from these statistical sets.

Analysis of these simulated data is presented in Figure 3. The original direction of the simulated wave is well reproduced by all the methods when the SNR is high, and, as we expect, the Poynting vector is found nearly parallel to $\mathbf{B_0}$. Values of $n/|Z|$ directly correspond to the cold plasma dispersion relation ($n$=6), because a unity transfer function $Z$ is supposed. For the same reason, we obtain zero phase shift $\Phi_b$. However, when the amplitude of the broadband noise becomes higher, the analysis results start to deviate from the initial values. This is manifested by increasing standard deviations of the results which indicate the level of expected random fluctuations. More importantly, the mean values of some parameters also change under the influence of the random noise. This is especially the case of the deviation of the Poynting vector from $\mathbf{B_0}$, whose mean value moves to 90° for noisy data. Both estimates of $D_b$ move to zero values, but the fluctuations are much more important for the method which involves the reconstruction of the full electric field vector. The fluctuations also become very high in the case of the $\Phi_b$ estimate.

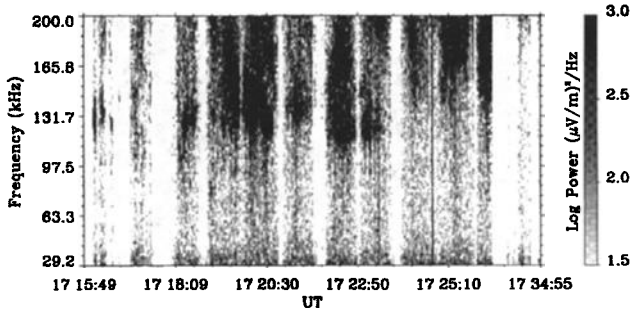



**Figure 4.** Power spectrogram of electric field data recorded in the HF band on November 10, 1996.

Comparing the results in Figure 2 with these simulations, we can see that for SNR around 0.1 both results may agree. The highly deviated Poynting vector may be explained by the shift of its mean value seen in the simulations. The occasional reversals of the sign of its parallel component are consistent with the high level of simulated fluctuations. Similar conclusions can be drawn concerning the $\Phi_b$ values. The values obtained from the experimental data for $n/|Z|$ are near the theoretically predicted refractive index of a cold plasma. This is also consistent with the simulations because the mean value of the simulated estimates is rather stable. The SNR value around 0.1 seems to be very low, but it should be noted that the simulated noise is broadband, and the signal is calculated at a fixed frequency. As we cannot reproduce statistical properties of the noise and their combination with the analysis bandwidths, we are not able to make any conclusions from the obtained SNR value. We can only qualitatively indicate that the noise may influence the results in a similar manner as we are observing with the experimental data.

### 3.2. Analysis of the Auroral Kilometric Radiation

The second example case concerns AKR observations in the HF band of MEMO on November 10, 1996. The spectrogram in Figure 4 shows intense broadband AKR emissions with a low-frequency cutoff varying between 100 and 130 kHz. The waveform measurements of three magnetic components and one electric component give data organized in snapshots of 0.009 s. The most intense signal was observed at 1719:45 UT, when the satellite was at invariant latitude of 71.2°, at 0318 MLT, and at an altitude of 19,182 km. A detailed analysis of the corresponding snapshot is presented in Figure 5. The AKR emission is seen in the interval from 137 kHz to ~162 kHz, just between two disturbing interference signals appearing in the magnetic field data. The polarization analysis of the wave magnetic field reveals that in all the frequency range, we observe right-hand nearly circularly polarized waves with a high polarization degree. The waves thus propagate in the *R-X* mode, and the plane wave approximation may be used. Figure 5e shows that the wave vector is inclined by 30°– 40° from $\mathbf{B}_0$, but the method of *Means* [1972] does not give any indication on whether we observe down-going or up-coming waves.

This is provided by parameters $D_a$ (Figure 5f) and $\Phi_a$ (Figure 5g), which take into account the electric signal. Both parameters indicate upward propagation in all the frequency range of the AKR. However, the conditions of validity of these estimations may not be fulfilled for the *R-X* mode. At AKR frequencies the parallel component of the wave electric field cannot be neglected, and the validity of analysis results depends on a relative angle deviation of the antenna from the wave vector. Figure 6 shows simulation results validating the analysis made for the case of November 10, 1996. The simulation has been made for the *R-X* mode, with all the characteristic frequencies well below ($f_g = 23$ kHz, $f_p = 10$ kHz) the selected wave frequency of 150 kHz. The wave vector direction has been defined following the observations at $\theta = 145°$. The simulated waveforms have been corrupted by a broadband Gaussian noise with SNR=3. The results show that the influence of the broadband noise is negligible

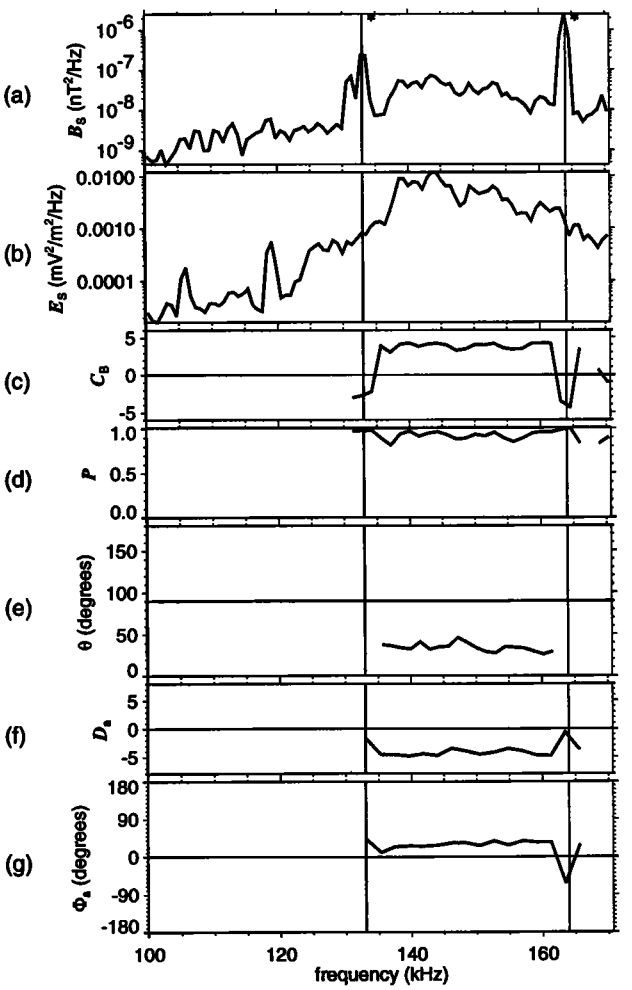



**Figure 5.** Analysis in the frequency interval 100 – 170 kHz in the HF band. Data were recorded on November 10, 1996, from 1719:45 UT. (a) Sum of the three magnetic autopower spectra; vertical lines and asterisks mark interference signals. (b) Autopower spectrum of the electric component. (c) Sense of polarization in the plane perpendicular to $\mathbf{B}_0$ from (4). (d) Degree of polarization from (5). (e) Deviation $\theta$ of the wave vector direction from the ambient magnetic field $\mathbf{B}_0$ by the method of *Means* [1972]. (f) Estimate of the parallel component of the Poynting vector normalized by its standard deviation from (7). (g) Phase shift from (6).

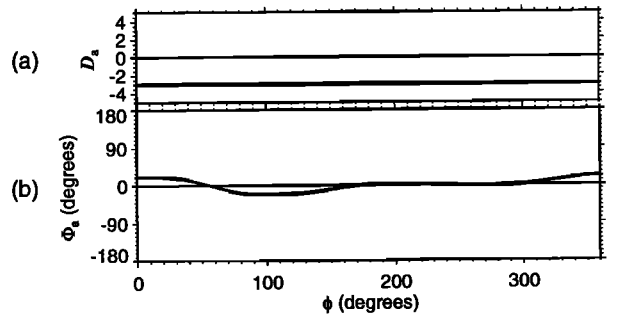



**Figure 6.** Analysis at 150 kHz as a function of angle azimuth $\phi$ of a simulated *R-X* mode wave. (a) Estimate of the parallel component of the Poynting vector normalized by its standard deviation from equation 7. (b) Phase shift between the electric signal and the perpendicular magnetic component from equation 6. The results are averaged from 100 independent realizations of the data with SNR=3.

and that both the $\Phi_a$ and $D_a$ parameters well reproduce the hemisphere of propagation.

## 4. Discussion

Analysis of the ELF case of November 12, 1996, shows high inclinations of the Poynting vector from $\mathbf{B_0}$. This apparently disagrees with the theory. We have shown that in this particular experimental situation, the results may be explained by the influence of the background noise on the results. The problem may however be also connected to the plasma model that we use for theoretical calculations. First, we must assume a value for the unknown plasma frequency. In a plasma of low density, the value of the plasma frequency may substantially influence whistler mode propagation and the Poynting vector may be found at large angles from $\mathbf{B_0}$. This is possible when the wave frequency becomes lower than the local lower hybrid frequency $f_{lh}$. However, given the measured gyrofrequency value, $f_{lh}$ cannot be higher than 555 Hz in an infinitely dense plasma. Therefore the frequency band of the observed emission always is above $f_{lh}$, whatever is the plasma frequency. The explanation given in section 3.1 seems then to be the only possible one in the frame of the linear theory of cold plasma. This theory also predicts a whistler mode refractive index which is very near to the experimentally obtained values.

Whistler-mode auroral hiss observed at high altitudes is often considered to be generated by the Landau resonance with auroral electron beams [*Gurnett et al.*, 1983]. In our case, the presence of the resonance cone and the observed high $\theta$ values indicate a similar generation mechanism. As the waves propagate downward, they may be generated by a resonant interaction with a beam of down-going electrons.

In Figure 7, simultaneously recorded data of the ION particle analyzer [*Sauvaud et al.*, 1998] show electrons at energies of several keV. These electrons probably originate in the plasma sheet, and their energy gradually increases as the satellite moves toward lower magnetic latitudes, from 70.9° at 1600 UT to 66.3° at 1640 UT. Near the point of observation of the bursts of ELF waves, we observe maximum electron fluxes around 1 keV, and at lower latitudes, the electron energies increase up to 3-4 keV. We also observe some fraction of electrons at energies around 200 eV.

However, there is no clear modulation of the electron energy spectra connected to pitch angle, and we have no direct evidence for field-aligned beams. Even if we do not find unstable electron distribution functions, it is not in contradiction with the generation mechanism that we propose. We observe electromagnetic waves that propagate from a distant region above the satellite, and free energy of the unstable source population has probably been already dissipated into the waves. The emissions are very bursty, and we cannot suppose a quasi-static equilibrium which could conserve some features of the original distribution function. The electrons we observe may however have similar energies as the source population. For 4-keV, 1-keV, and 200 eV field-aligned electrons, the Landau resonance condition is satisfied for waves with parallel refractive indices of 8, 16, and 36, respectively. These values may be reached near the whistler mode resonance cone. Indeed, such generation mechanism has been reported by *Ergun et al.* [1993] who observed enhanced short-wavelength VLF emissions occurring during dispersive bursts of low-energy electron fluxes. The measurements were made in the auroral ionosphere, and electrostatic waves were observed on the whistler mode resonance cone with a parallel refractive index of 17. Under these conditions, unstable features have been identified in the electron distribution function.

It is widely thought that AKR originates from the relativistic gyroresonant interaction with loss cone distribution of upgoing electrons, as proposed by *Wu and Lee* [1979]. According to this model, we will suppose generation at frequencies around the local electron gyrofrequency. The lower cutoff of intense emission of AKR corresponds then to the highest source altitude. As this cutoff is found at 137 kHz (see Figure 5) and the local electron gyrofrequency is only 23 kHz, the source must be confined well below the obser-

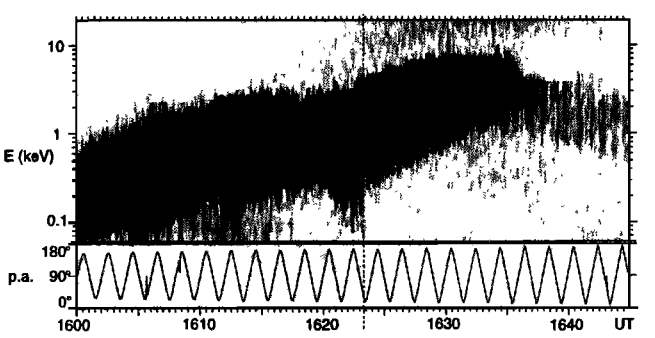



**Figure 7.** (top) Energy spectrogram of electrons between 60 eV and 20 keV detected by the ION experiment on November 12, 1996, as a function of UT. Shading indicates the count rate between 0 and 1000 counts $s^{-1}$. (bottom) Pitch angle of analyzed electrons. The vertical dashed line shows the position of the bursty ELF emissions observed by MEMO.

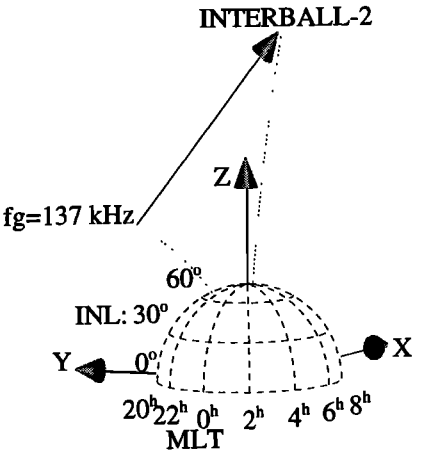



**Figure 8.** Projection of the wave vector direction of AKR back to the source region. Axes $X$, $Y$, and $Z$ of the solar magnetic (SM) coordinate system are indicated by arrows. The Earth's surface is marked by parallels at constant invariant latitude (INL) and by meridians at constant magnetic local time (MLT). The wave vector is given by an arrow pointing toward the satellite position (tip of the arrow, marked INTERBALL-2). The other side of the arrow indicates a place where the local $f_g$ reaches 137 kHz. The corresponding magnetic lines of force passing through the satellite position and through the possible source region are plotted by dotted lines.

vation point at an altitude of 19,182 km. We thus expect to observe upward propagation in the entire frequency range. This is really confirmed by propagation analysis in Figure 5. Other results of our analysis show that AKR propagates in the *R-X* mode as a plane wave inclined by 140°– 150° from the Earth's magnetic field. The azimuth $\phi$ is found between 70° and 100° (not shown in Figure 5), indicating propagation from lower MLT and lower latitudes. Figure 8 shows a projection of the wave vector back toward the source region. We suppose a negligible refraction, and we follow the direction opposite to the average wave vector direction between 137 and 162 kHz ($\theta = 146°$, $\phi = 86°$). As we go down in altitude and invariant latitude, the electron gyrofrequency increases, and on auroral filed lines, it falls into the frequency interval of the observed AKR emission. The lower cutoff frequency at 137 kHz becomes equal to the local gyrofrequency at an altitude of 7750 km, invariant latitude of 51.1°, and on 2204 MLT. Footprint of the corresponding field line on the Earth's surface is at invariant latitude of 62.1° and on 2231 MLT. Note that we use a simple dipolar model of the magnetic field in this example. Note also that the position of the estimated source region is highly sensitive to the initial $\theta$ value. If we for example use the method of *McPherron et al.* [1972] instead of the method of *Means* [1972], we obtain an average $\theta$ of 151°, and the above condition for the cutoff frequency is reached at a higher altitude and invariant latitude, and on a slightly different MLT (8120 km, 63°, and 2229 MLT, respectively). These values move the corresponding field line footprint up to an invariant latitude of 69.7°, and to 2258 MLT. A detailed examination of this problem is beyond the scope of the present paper. However, all these results are roughly consistent with previous findings on AKR propagation known from DE-1 and Viking data [e.g., *Gurnett et al.*, 1983; *Calvert and Hashimoto*, 1990; *Le Quéau and Louarn*, 1996]. After WDF analysis of MEMO data by *Parrot et al.* [2001], our results represent the first direct determination of the complete wave vector direction at AKR frequencies. We use here completely independent plane-wave methods, and the fact that we may confirm previously obtained results shows the potential of the above presented techniques for future analyses.

## 5. Conclusions

1. We have described several methods for wave propagation analysis based on simultaneous measurement of several field components. Under some conditions we can determine the complete wave vector direction from three magnetic field components and a single electric field component. With three magnetic and two electric components we can characterize the complete wave vector direction, wave refractive index, and the transfer function of the antenna-plasma interface. Moreover, the missing electric component may be estimated, and the Poynting vector can be determined.

2. The above analysis techniques can be used to describe wave fields which are near to a single plane wave in a single wave mode. If any of these conditions is violated, the results must be verified by the WDF methods.

3. Application to multicomponent waveform data measured by the MEMO device onboard INTERBALL-2 in the nightside auroral region shows that whistler mode bursty ELF emission observed on November 12, 1996, propagates in the whistler mode at wave vector directions near to the Gendrin angle and not far from the resonance cone. The waves propagate from the nightside sector toward the Earth, in the direction of growing magnetic latitude. Their source must then be at auroral latitudes above 18,300 km. The generation mechanism is probably connected with plasma sheet electrons which are observed at the same time as the ELF bursts.

4. As the second example, we analyse *R-X* mode AKR emission observed on November 10, 1996. The results show that the waves are upgoing with wave vector directions inclined by 140°– 150° from $\mathbf{B}_0$, consistently with their generation near the local electron gyrofrequency in the auroral region. After the paper of *Parrot et al.* [2001], where the WDF methods have been used, this is the first similar verification done by plane wave methods directly from the electric and magnetic waveform data. Both these examples demonstrate a great potential of such kind of analysis for future applications.

## Appendix A: Estimation of the Full Electric Field Vector Using the Magnetic Field Vector Data and Two Electric Signals

The Faraday's law in the frequency domain may be used to reconstruct the electric field vector from the magnetic

field vector data and two electric components [*Grard*, 1968; *Shawhan*, 1970]. If the data are known in a form of averaged spectral matrices (2), they must be first transformed back to the complex amplitudes $\mathcal{A}_i$ of separate signals. We can define them as

$$\mathcal{A}_i = \sqrt{S_{ii}}\, e^{i\varphi_i}, \tag{A1}$$

where $S_{ii}$ is the autopower spectrum of the respective signal $i$ and $\varphi_i$ is a phase obtained from complex phases $\pi_{ij}$ of all concerned cross-power spectra $S_{ij}$,

$$\varphi_i = \frac{1}{m}\left[-2\pi_{1i} - \sum_{j=2}^{i-1}(\pi_{ji} + \pi_{1j}) + \sum_{j=i+1}^{m}(\pi_{ij} - \pi_{1j})\right], \tag{A2}$$

taking $i$ from 2 to $m$ ($m = 5$ is the total number of signals) and defining $\varphi_1 = 0°$. As the phases $\pi_{ij}$ arise from $S_{ij} = |S_{ij}| \exp i\pi_{ij}$, the cyclic nature of all terms in (A2) must be taken into account when doing the summation. This equation is obtained by a least squares method from an overdetermined system of equations involving all the $(m^2 - m)/2$ cross spectra to determine $m - 1$ relative phases. This operation, however, does not lead to the loss of information only in the case of absolutely coherent spectral matrix exactly corresponding to a single plane wave. Otherwise, we lose the information about the relative coherences estimated by averaging the spectral matrix in (2).

The real and imaginary parts of the third electric component may be then calculated using the condition of perpendicularity of the wave electric and magnetic fields derived from (9),

$$\begin{aligned} \Re E_{z'} &= -\frac{\Re B_{x'}\,\Re E_{x'} + \Re B_{y'}\,\Re E_{y'}}{\Re B_{z'}}, \\ \Im E_{z'} &= -\frac{\Im B_{x'}\,\Im E_{x'} + \Im B_{y'}\,\Im E_{y'}}{\Im B_{z'}}, \end{aligned} \tag{A3}$$

where the complex amplitudes $B_{x'}$, $B_{y'}$, $B_{z'}$, $E_{x'}$, and $E_{y'}$ are calculated with (A1) and transformed to the Cartesian frame defined by the two electric antennas (see above). Obviously, we can use (A3) only if the $B_{z'}$ component has a nonnegligible magnitude, i.e., if the wave magnetic field is polarized out of the plane of the electric antennas. Whenever this is the case, we can manage nonzero values of $\Re B_{z'}$ and $\Im B_{z'}$ by shifting the phases of all components by an appropriate constant angle. Finally, the six wave field components may be transformed back to the $\mathbf{B_0}$ frame, and a spectral matrix 6×6 may be calculated by (2).

With this spectral matrix, we have complete information about the wave electric and magnetic fields. It can be used by different analysis methods. For instance, we can extend (8) for three electric signals or we can estimate the average Poynting vector,

$$\begin{aligned} F_x &= \frac{1}{2\mu_0}\left(S_{EyBz} - S_{EzBy}\right), \\ F_y &= \frac{1}{2\mu_0}\left(S_{EzBx} - S_{ExBz}\right), \\ F_z &= \frac{1}{2\mu_0}\left(S_{ExBy} - S_{EyBx}\right), \end{aligned} \tag{A4}$$

where we suppose the absence of spatial dispersion (cold plasma approximation) and where $\mu_0$ is the vacuum permeability.

**Acknowledgments.** Many thanks are due to J.A. Sauvaud and H. Stenuit who provided us with the data of the ION particle analyzer, and to J.Y. Brochot who helped us with the processing of MEMO data. This work was supported by the French-Czech program Barrande 98039/98055 and by the international program of scientific cooperation (PICS) 469 with the joint Czech Grant Agency grant 205/01/1064. O. Santolík acknowledges the support of the Czech Grant Agency grant 205/00/1686.

Janet G. Luhmann thanks the referees for their assistance in evaluating this paper.

## References

Calvert, W., and K. Hashimoto, The magnetoionic modes and propagation properties of auroral radio emissions, *J. Geophys. Res., 95*, 3943–3957, 1990.

Ergun, R.E., G.T. Delory, E. Klementis, C.W. Carlson, J.P. McFadden, I. Roth, and M. Temerin, VLF wave growth from dispersive bursts of field-aligned electron fluxes, *J. Geophys. Res., 98*, 3777–3787, 1993.

Grard, R., Interprétation de mesures de champ électromagnétique T.B.F. dans la magnétosphère, *Ann. Geophys., 24*, 955–971, 1968.

Gurnett, D.A., S.D. Shawhan, and R.R. Shaw, Auroral hiss, Z mode radiation, and auroral kilometric radiation in the polar magnetosphere: DE 1 observations, *J. Geophys. Res., 88*, 329–340, 1983.

Lefeuvre, F., Y. Marouan, M. Parrot, and J.L. Rauch, Rapid determination of the sense of polarization and propagation for random electromagnetic wave fields. Application to GEOS1 and AUREOL3 data, *Ann. Geophys., 4*, 457–468, 1986. (Correction, *Ann. Geophys., 5*, 251, 1987.)

Lefeuvre, F., J.L. Rauch, D. Lagoutte, J.J. Berthelier, and J.C. Cerisier, Propagation characteristics of dayside low-altitude hiss: case studies, *J. Geophys. Res., 97*, 10,601–10,620, 1992.

Lefeuvre, F., M. Parrot, J.L. Rauch, B. Poirier, A. Masson, and M. Mogilevsky, Preliminary results from the MEMO multicomponent measurements of waves on-board INTERBALL 2, *Ann. Geophys. 16*, 1117–1136, 1998.

Louarn, P., and D. Le Quéau, Generation of the auroral kilometric radiation in plasma cavities, II, The cyclotron maser instability in small size sources, *Planet. Space Sci., 44*, 211–224, 1996.

Means, J. D., Use of the three-dimensional covariance matrix in analyzing the polarization properties of plane waves, *J. Geophys. Res., 77*, 5551–5559, 1972.

McPherron, R. L., C. T. Russel, and P. J. Coleman Jr., Fluctuating magnetic fields in the magnetosphere, 2, ULF waves, *Space Sci. Rev., 13*, 411–454, 1972.

Parrot, M., F. Lefeuvre, and Y. Marouan, On the direct identification of propagation modes for HF plasma waves, *J. Geophys. Res., 94*, 17,049 – 17,062, 1989.

Parrot, M., F. Lefeuvre, J.L. Rauch, O. Santolík, and M.M. Mogilevski, Propagation characteristics of AKR observed by the MEMO experiment onboard INTERBALL-2, *J. Geophys. Res.*, in press, 2001.

Priestley, M. B., Spectral analysis and time series, Academic, San Diego, Calif., 1989.

Samson, J. C., Matrix and Stokes vector representations of detectors for polarized waveforms: Theory, with some applications to teleseismic waves, *Geophys. J. R. Astron. Soc., 51*, 583-603, 1977.

Samson, J. C., and J. V. Olson, Some comments on the descriptions of the polarisation states of waves, *Geophys. J. R. Astron. Soc., 61*, 115–129, 1980.

Santolík, O., Propagation analysis of STAFF-SA data with co-

herency tests, *rep. LPCE/NTS/073.A*, Lab. Phys. Chimie Environ./CNRS, Orléans, France, 2000.

Santolík, O., and M. Parrot, Propagation analysis of electromagnetic waves between the helium and proton gyro-frequencies in the low-altitude auroral zone, *J. Geophys. Res., 103*, 20,469–20,480, 1998.

Santolík, O., and M. Parrot, Case studies on wave propagation and polarization of ELF emissions observed by Freja around the local proton gyro-frequency, *J. Geophys. Res., 104*, 2459–2476, 1999.

Santolík, O., and M. Parrot, Application of wave distribution function methods to an ELF hiss event at high latitudes, *J. Geophys. Res., 105*, 18,885 – 18,894, 2000.

Sauvaud, J.A., H. Barthe, C. Aoustin, J.J. Thocaven, J. Rouzaud, E. Penou, D. Popescu, R.A. Kovrazhkin, and K.G. Afanasiev, The ion experiment on board the Interball-Auroral satellite: Initial results on velocity-dispersed structures in the cleft and inside the auroral oval, *Ann. Geophys., 16*, 1056-1069, 1998.

Shawhan, S. D., The use of multiple receivers to measure the wave characteristics of very-low-frequency noise in space, *Space Sci. Rev., 10*, 689–736, 1970.

Stix, T. H., *Waves in Plasmas,* Am. Inst. of Phys., New York, 1992.

Storey, L. R. O., and F. Lefeuvre, The analysis of 6-component measurement of a random electromagnetic wave field in a magnetoplasma, 1, The direct problem, *Geophys. J. R. Astron. Soc., 56*, 255–270, 1979.

Storey, L. R. O., F. Lefeuvre, M. Parrot, L. Cairó, and R. R. Anderson, Initial survey of the wave distribution functions for plasmaspheric hiss observed by ISEE 1, *J. Geophys. Res., 96*, 19,469–19,489, 1991.

Wu, C. S., and L. C. Lee, A theory of the terrestrial kilometric radiation, *Astrophys. J., 230*, 621–626, 1979.

F. Lefeuvre, M. Parrot, and J.L. Rauch, Laboratoire de Physique et Chimie de l'Environnement, CNRS, 3A, Avenue de la Recherche Scientifique, F-45071 Orléans cedex 02, France. (lefeuvre@cnrs-orleans.fr; mparrot@cnrs-orleans.fr; jlrauch@cnrs-orleans.fr)

O. Santolík, Faculty of Mathematics and Physics, Charles University, V Holešovičkách 2, CZ-18000 Praha 8, Czech Republic. (ondrej.santolik@mff.cuni.cz)

(Received July 13, 2000; revised November 14, 2000; accepted November 14, 2000.)